APPLICATIONS OF
MODELLING AND SIMULATION
http://arqiipubl.com/ams eISSN 2600-8084 VOL 9, 2025, 37-50

Optimizing Invasive ECT Sensor Dimensions for Conducting Pipe: A Simulation Study

Ain Eazriena Che Man[1], Yasmin Abdul Wahab[1*], Nurhafizah Abu Talip Yusof[1,2], Suzanna Ridzuan Aw[3], Mohd Mawardi Saari[1], Ruzairi Abdul Rahim[4,5] and Sia Yee Yu[6]

[1]Faculty of Electrical & Electronics Engineering Technology, Universiti Malaysia Pahang Al-Sultan Abdullah, 26600 Pekan, Pahang, Malaysia
[2]Centre for Research in Advanced Fluid & Processes (Fluid Centre), Universiti Malaysia Pahang Al-Sultan Abdullah, Lebuhraya Tun Razak, 26300 Gambang, Kuantan, Pahang, Malaysia
[3]Faculty of Engineering Technology (Electrical & Automation), University College TATI, 24000, Jalan Panchor, Telok Kalong, 24000 Kemaman, Terengganu, Malaysia
[4]Process Tomography Research Group (Protom-i), Faculty of Electrical Engineering, Faculty of Engineering, Universiti Teknologi Malaysia, 81310 UTM Skudai, Johor, Malaysia
[5]Faculty of Electrical and Electronic Engineering, Universiti Tun Hussein Onn Malaysia, 86400 Parit Raja, Batu Pahat, Johor, Malaysia
[6]LOGO Solution Sdn. Bhd., Wisma SP Setia, Jalan Indah 15, Bukit Indah, 79100 Iskandar Puteri, Johor, Malaysia

*Corresponding author: yasmin@umpsa.edu.my

Submitted 02 August 2024, Revised 18 October 2024, Accepted 27 October 2024, Available online 04 January 2025.

Abstract: This simulation study aims to optimize the dimensions of an invasive Electrical Capacitance Tomography (ECT) sensor for conducting pipe applications. Conventional non-invasive ECT techniques are ineffective for conducting pipes, as they cannot penetrate the pipe wall. This study explores the use of an invasive ECT system to identify homogeneous and non-homogeneous dielectric media within conducting pipes. A simulation model is developed using the finite element method (FEM) and the Linear Back Projection (LBP) algorithm for image reconstruction, further enhanced by a global threshold method. Various sensor dimensions are tested in a 150 mm length steel pipe, with a sinusoidal waveform source of 25 Vpp and a frequency of 400 kHz applied to the model in both homogeneous and non-homogeneous dielectric media conditions. The simulation results reveal that the sensitivity and resolution of the invasive ECT system are significantly influenced by the sensor dimensions. Optimal sensor dimensions indicate that longer and wider sensors, covering approximately 80% of the sensor coverage area and 60% of the pipe length, provide higher electrical voltage and better resolution. Overall, this study provides valuable insights into optimizing invasive ECT sensor dimensions for observing dielectric media inside conducting pipes, significantly improving the accuracy and reliability of industrial process monitoring in both homogeneous and non-homogeneous media.

Keywords: Conducting pipe; Dielectric; Electrical Capacitance Tomography; Invasive; Tomography.

1. INTRODUCTION

A useful imaging method for examining the dielectric medium inside different objects is Electrical Capacitance Tomography (ECT). Through the measurement of capacitance fluctuations between electrodes placed on the inner (invasive approach) or outer (non-invasive technique) surface of a pipe, ECT allows for the viewing of the distribution and dynamics of the dielectric medium in real-time. However, the ECT sensor's design parameters have a significant impact on the ECT imaging's resolution and accuracy. More specifically, the sensor's imaging performance is greatly influenced by its length and width. Achieving high-resolution imaging while retaining sensitivity to variations in the dielectric medium requires optimizing these dimensions.

Conducting pipes are used to transfer a variety of commodities in numerous industries, including food production, chemical processing, and oil and gas. Precise observation and description of the medium within these pipes are essential. Conventional non-invasive ECT methods, as examples in Ref. [1–6], are unsuitable for steel pipes because the metal sensors placed outside the pipe cause the electrical signal cannot penetrate the conducting material. Moreover, operators can guarantee the integrity and effectiveness of pipeline systems, identify anomalies like gas pockets or liquid slugs, and obtain important insights into flow patterns by using an invasive ECT sensor. Similar to this, invasive ECT sensors in chemical processing enable direct medium measurement, facilitating phase separation detection and flow distribution optimization, both of which improve production efficiency.

Optimizing sensor width and length is critical because conducting pipes have unique requirements for monitoring dielectric medium. Many studies have been conducted in the past on ECT sensor improvement. For instance, authors in [7] examined how various electrode sizes affect permittivity detection by analysing the performance of 16-electrode sensor designs for a 17 mm diameter sensing zone. A unique design for an ECT sensor with variable diameter that is appropriate for concrete pole inspection was validated by [8]. Important ECT sensor design considerations, like electrode length and number and usage of internal and exterior electrodes, were covered in [9].

Other research, such as that conducted by [10] and [11], concentrated on axial electrode length optimization and the knowledge of the linked aspects impacting the quality of ECT imaging. The impact of sensor length on fluidized bed measurements was investigated by Kai Huang et al. [12], and the results showed that it had a major effect on bubble detection. Nonetheless, the majority of these investigations concentrated on non-invasive methods and non-conductive pipe materials.

The goal of this simulation study is to use an invasive method inside conducting pipes to optimize the length and width of ECT sensors. Through an examination of distinct elements peculiar to conducting pipes, this research aims to offer significant perspectives and recommendations for the development of ECT sensors customized for industrial use. This study models an ECT sensor with an oil dielectric medium and a 25 Vpp source and 400 kHz frequency in a 150 mm steel pipe using the finite element method (FEM) and the linear back projection (LBP) technique. A global threshold approach is used to improve image reconstruction and a variety of sensor dimensions are examined. The findings are anticipated to have a big impact on the oil and gas, chemical, and food processing industries, where precise and non-destructive material flow monitoring is essential to preserving product quality and safety.

2. BASIC PRINCIPLE OF INVASIVE ECT SYSTEM

An ECT sensor is used to measure the permittivity distribution inside an object in ECT [13]. The amount of charge needed to produce a unit potential difference between a capacitor's plates is known as its capacitance [14]. Equation (1) can be used to illustrate the relationship between the capacitance, C, and the spatial permittivity, ε value. The electric constant is represented by ε_0, the size of the sensing electrode is by A, and the distance between one pair of electrodes is by d [15].

$$C = \frac{\varepsilon_o \varepsilon A}{d} \tag{1}$$

The main idea of this simulation study is to place a number of conducting plates, or electrodes, around the vessel's edge. It is possible to measure the differences in capacitance between several pairs of electrodes by inserting a dielectric material within the vessel [5, 16, 17]. This measuring procedure is carried out for various combinations of electrodes in order to gather information that will aid in reconstructing the permittivity distribution inside the sensor [18]. Equation (2) illustrates how Poisson's equation can be used to derive the relationship between the measured capacitances and the spatial distribution of permittivity.

$$\nabla \cdot (\varepsilon(x,y,z) \cdot \nabla\varphi(x,y,z)) = 0 \tag{2}$$

where ε is the spatial permittivity distribution and φ is the electric field potential distribution within the sensor. For a three-dimension case that involving x, y and z axes, the relative permittivity distribution $\varepsilon(x,y,z)$ is considered. This distribution is defined within the boundary conditions, $\varphi = VC$ for the first electrode and $\varphi = 0$ for the remaining electrodes. Hence, this three-dimensional approach was considered in the ECT system modelling to mimic the real hardware of ECT system.

3. METHODOLOGY

3.1 Sensor Arrangement Strategy

This invasive ECT system's sensor arrangement is comparable to the conducting boundary technique seen in electrical resistance tomography (ERT) devices, as mentioned in [19]. The main purpose of this configuration is to avoid direct short-circuit contact between the conducting materials - that is, the conducting pipe and the metal electrode. The system operates by introducing an electric potential difference between two adjacent electrodes, while voltage measurements are taken across consecutive pairs of neighbouring electrodes. Each pair of electrodes is sequentially designated as transmitter (Tx) and receiver (Rx), with a 25 Vpp, 400 kHz sinusoidal waveform applied as the source (Tx) to one electrode and the other set as the receiver (Rx). The 400 kHz was selected based on the result in Ref. [20]. The electrode pair where the electrical potential is injected is sequentially switched to the next set of electrodes until all possible combinations of independent measurements have been performed. Figure 1 illustrates the geometry of the model ECT system in 2-dimensional terms with an example where Electrode 1 (E1) is set as the transmitter or source (Tx) and Electrode 2 (E2) is set as the receiver (Rx).

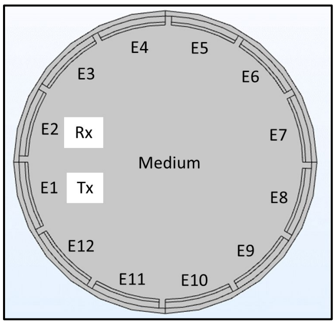

Figure 1. Example of one pair of electrodes (E1 is set as transmitter or source (Tx) and E2 is set as receiver (Rx).

This process continues until a complete set of 12 pairs of electrodes (E1, E2, ..., E12) as shown in Table 1 is measured. In total, 132 data measurements or 66 independent measurement data points are obtained for this model. Subsequently, an image of the object or material distribution is reconstructed using these measurements. The formula for this measurement strategy, M is expressed by Equation (3) [21] where N is the total number of electrodes.

$$M = \frac{N(N-1)}{2} \tag{3}$$

Table 1. Measurement strategy for conducting boundary.

Transmitter (Tx) / Receiver (Rx)	E1	E2	E3	E4	E5	E6	E7	E8	E9	E10	E11	E12	No. of Measurement
E1	x												11
E2		x											11
E3			x										11
E4				x									11
E5					x								11
E6						x							11
E7							x						11
E8								x					11
E9									x				11
E10										x			11
E11											x		11
E12												x	11
												Total Measurements	**132**

3.2 Modelling Geometry of ECT Sensor

The successful implementation and optimization of invasive ECT system require sophisticated modelling tools capable of simulating complex multi-physics phenomena. In this study, we focus on the modelling and optimization of an invasive ECT system using COMSOL Multiphysics software. COMSOL offers a versatile platform for simulating the intricate interactions of electric fields, material properties, and geometric configurations inherent in ECT systems. The 3-dimensional model was selected because it mimics the real hardware configuration. The number of electrodes selected in this study is selected based on research by [22] which is 12-electrode. It is assumed that the use of more electrodes in an electrical capacitance tomography (ECT) sensor would result in higher resolution images. However, research by [2] proved that 12-electrode ECT sensor is recommended for most applications as the research showed limited new information can be obtained and little improvement in the quality of images be achieved if the number of electrodes is more than 12. Table 2 and Figure 2 show the parameter and constructed geometry model of the proposed invasive ECT system where the electrodes are embedded in the shield guard to improve the performance of the sensor. The insulated layer and shield protection of this particular ECT sensor variant are integrated into the sensor itself. Figure 2 also shows the inside cross-section of each electrode as well as the sensor's schematic design. In order to avoid inaccurate sensor readings and poorer image quality, the shield guard is designed within the sensor to stop the electric field lines from expanding outside of the sensor's designated zone. As a result, before modelling the electrode width and length parameters, the shield guard's diameter is established. To reduce fringe effects, it is assumed that the shield guard diameter is greater than the electrode diameter.

Table 2. Parameters of invasive ECT model used.

Items	Parameters	Items	Parameters
Number of electrodes	12	Conducting pipe (Structural steel)	$\varepsilon = 1.0$
Diameter of pipe	100 mm	Insulated layer (Silicone)	$\varepsilon = 11.7$
Length of pipe	150 mm	Shield guard (FR4)	$\varepsilon = 1.0$
Thickness of pipe	1.8 mm	Electrode (Copper)	$\varepsilon = 6.0$
Thickness of electrodes	0.5 mm	Main medium (Oil)	$\varepsilon = 3.4$
Thickness of shield guard	1.0 mm	Phantom/bubble (Air)	$\varepsilon = 1.0$
Thickness of insulated layer	2.0 mm		

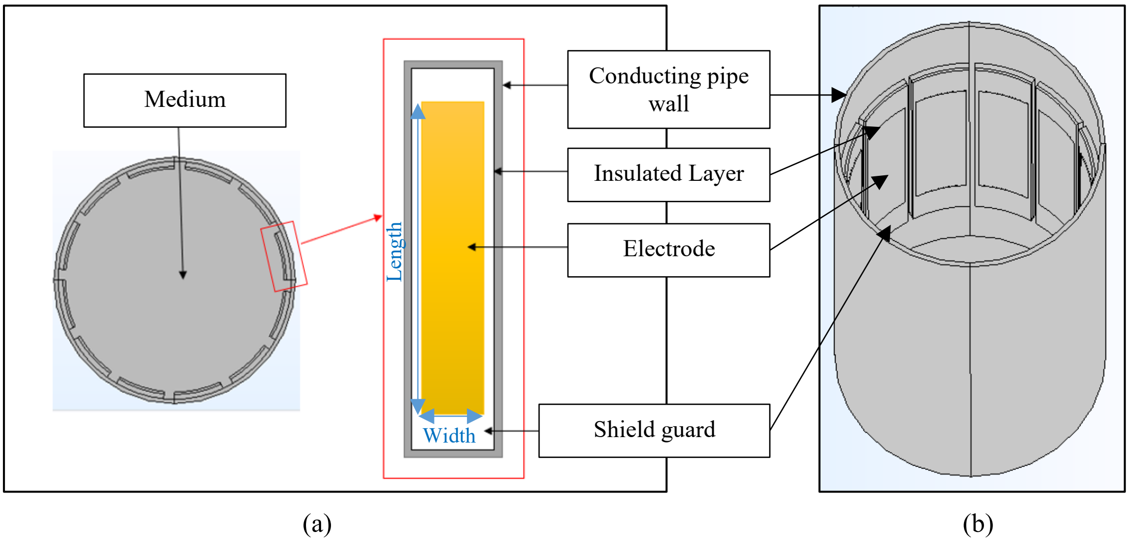

Figure 2. Invasive ECT model drawn in COMSOL Multiphysics software: (a) 2D view of the invasive ECT model with highlighting the electrode, (b) 3D view of the invasive ECT model.

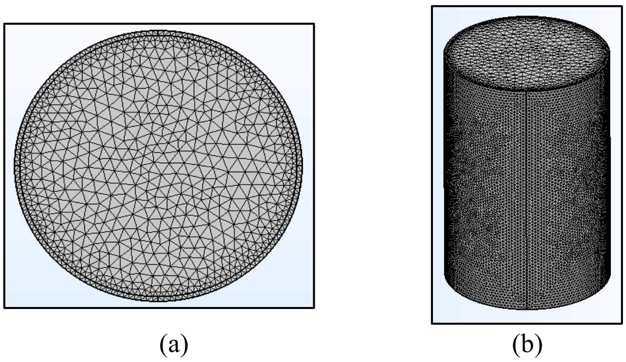

Figure 3. (a) 2D of generated meshed and (b) 3D of generated meshed.

Afterwards, the behaviour of electric fields in systems with stationary charges is simulated using the electrostatics module in COMSOL Multiphysics. To further comprehend the relationship between the electrodes and the substance being studied, the electrostatics module also makes it possible to model the distribution of the electric field inside the imaging region. The extra fine meshing setting is selected to provide more reliable numerical solution using the FEM simulation. Figure 3 shows the generated mesh of the system. Next, the results with the assigned width and length of the invasive model were investigated and analysed. The results and discussion in detail will be provided under Section 4.

3.3 Sensor Dimension Optimization

The length of the electrode is analyzed from 70 mm to 110 mm with an increment of 10 mm in the conducting pipe. Simultaneously, the width of the electrode is analyzed using the sensor coverage area implemented in the 360° circumferences of the conducting pipe, varied from 50% to 90% with an increment of 10%. To calculate the sensor coverage area (%) in COMSOL Multiphysics software, the (%) are converted to arc length (mm) and then converted to arc angles, θ by using the formula in Equation (4). Table 3 shows the value of the conversion of the width of the electrode based on sensor coverage area and electrode diameter that varied accordingly.

$$\theta = \frac{Sensor\ coverage\ area\ (\%)}{100} \times \left(\frac{360°}{Number\ of\ electrode}\right) \tag{4}$$

Besides, the gap of the shield guard and insulated layer from the electrode length is added by 20 mm at the top and bottom of the electrode while the width is increased by 1.5 mm at the left and right of the electrode. Then, it will vary accordingly based on the adjustment of electrode length and width. Figure 4 shows the diameter for shield guard and insulated layer which is larger than the diameter of the electrode and Table 4 shows the adjustment of the width of shield guard and insulated layer based on dimension of electrode. Consequently, Table 5 revealed the construction of the sensor geometry in the COMSOL Multiphysics software based on the adjusted sensor dimension. This variation of the model was used to obtain the results for the selection of the optimal dimension.

Table 3. Width of electrode.

Width (%)	Arc Length (mm)	Arc Angle, θ
50	12.85	15°
60	15.43	18°
70	18.00	21°
80	20.57	24°
90	23.14	27°

Table 4. Width of shield guard and insulated layer based on dimension of electrode.

Width (%)	Arc Length (mm)	Arc Angle, θ
50	15.85	18.5°
60	18.43	21.5°
70	21.00	24.5°
80	23.57	27.5°
90	26.14	30.5°

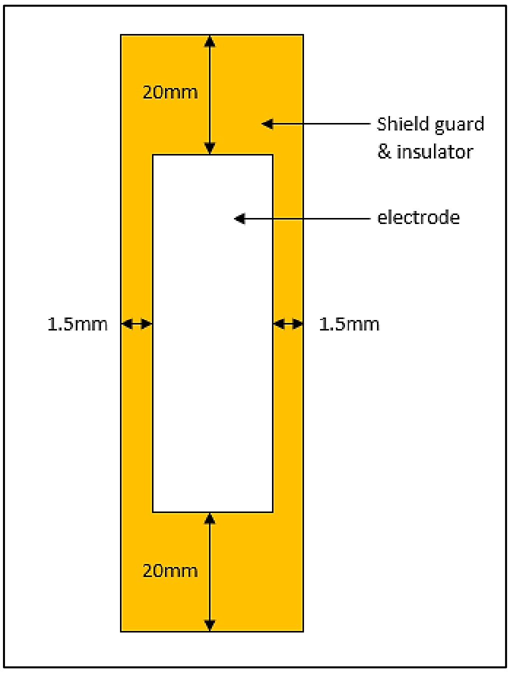

Figure 4. The initial diameter of shield guard and insulator that will be varied based on the adjustment of electrode length and width.

Table 5. The construction of the sensor geometry in the COMSOL Multiphysics software based on the adjusted sensor dimension.

Width of Sensor (%)	Length of Electrode (mm)				
	70	80	90	100	110
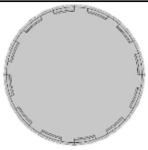 50%	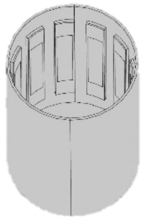	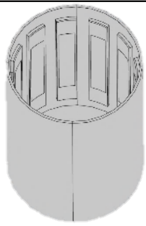	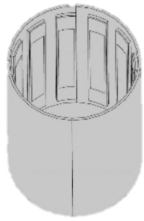	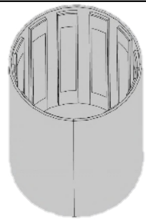	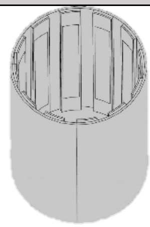
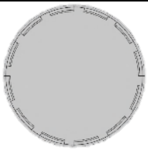 60%	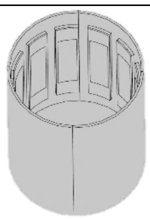	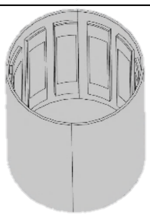	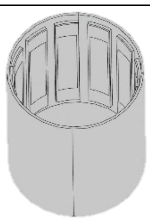	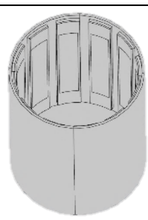	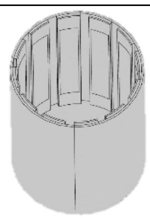
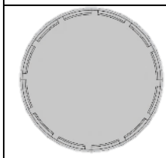 70%	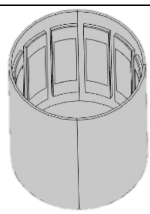	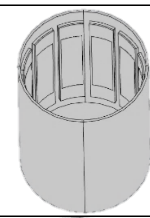	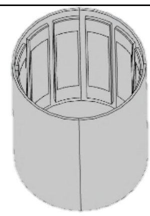	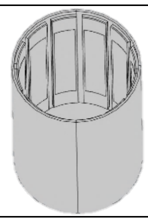	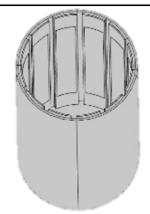
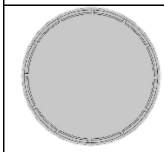 80%	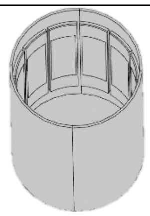	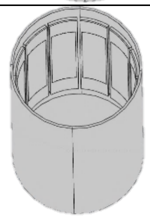	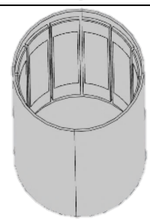	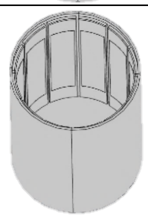	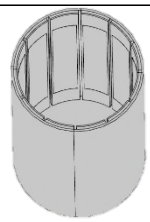
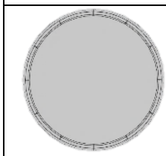 90%	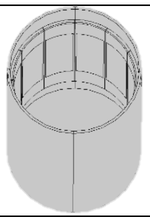	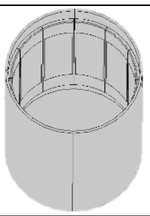	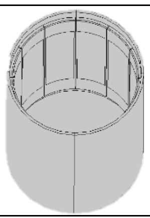	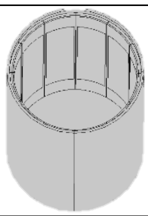	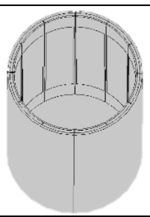

4. RESULTS AND DISCUSSION

The results obtained were analysed once the invasive ECT system's geometry was constructed. COMSOL Multiphysics software was used to get two separate electrode pairing measurements of the electrical potential values: opposing readings (E1 as Tx and E7 as Rx channels) and neighbouring readings (E1 as Tx and E2 as Rx channels) from the same invasive ECT system model. With these two arrangements, the goal is to ascertain which electrodes - the nearest (adjacent) or the farthest (opposite) - can achieve the highest voltage when the recommended invasive ECT system parameter is applied in the fully non-conducting medium condition, or homogenous condition. Table 6 shows the simulation results of homogenous medium with electrical voltage measurements in COMSOL Multiphysics software where width and length are analysed accordingly. The contour lines represented by the purple colour while the multislices line represented by the black colour. The curving pattern from both lines omit the soft field behaviour of the electrical tomography. Figure 5 illustrates the plot analysis of varied electrode width and length versus electrical voltage based on simulation result for both adjacent and opposite readings.

Table 6. Electrical potential distribution and values for adjacent and opposite measurement in homogenous medium with varied electrode width and length.

Length of Electrode (mm)/ Measurement (V)	**Width of Sensor (%)**				
	50	**60**	**70**	**80**	**90**
70	Top View				
	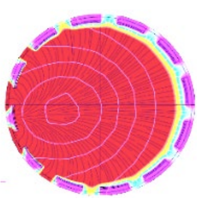	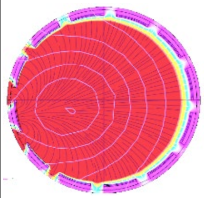	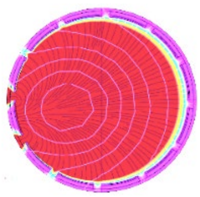	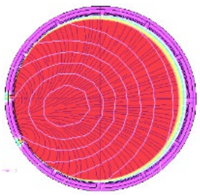	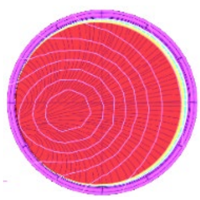
	3D View				
	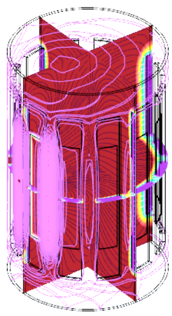	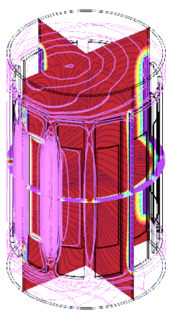	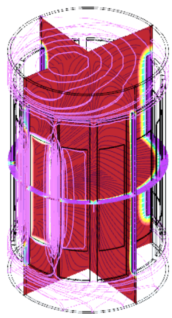	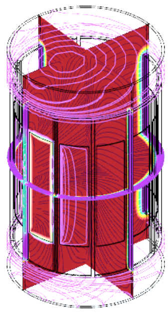	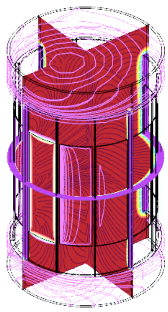
Adjacent	0.012101V	0.014294V	0.01735V	0.021861V	0.030633V
Opposite	5.28E-04V	5.83E-04V	6.46E-04V	7.18E-04V	8.13E-04V
80	Top View				
	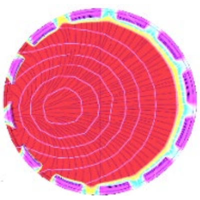	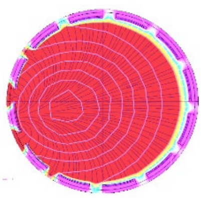	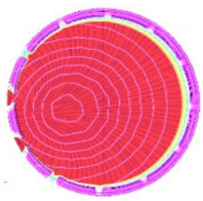	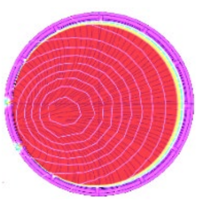	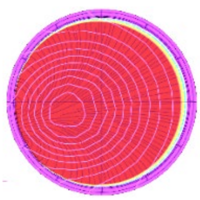
	3D View				
	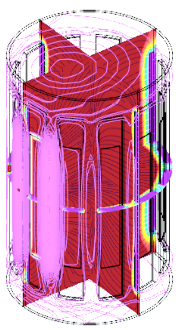	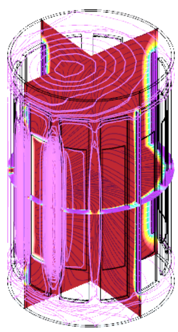	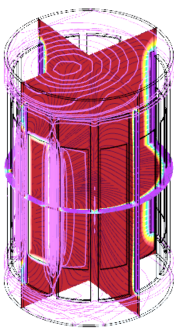	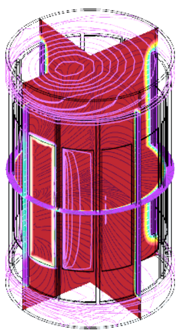	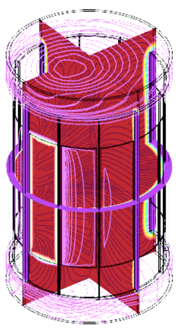
Adjacent	0.012361V	0.014577V	0.017707V	0.022356V	0.031211V
Opposite	5.63E-04V	6.22E-04V	6.91E-04V	7.70E-04V	8.71E-04V
	Top View				

90	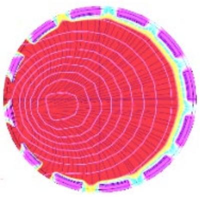	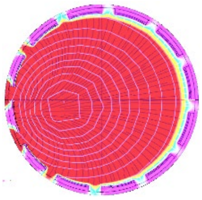	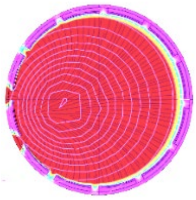	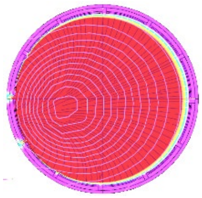	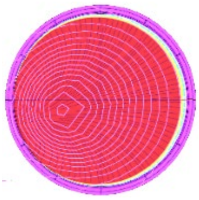
	3D View				
	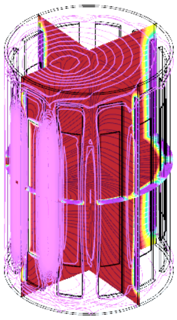	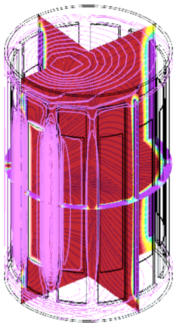	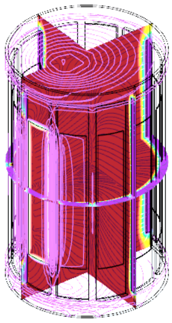	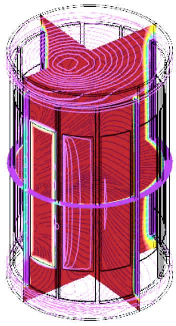	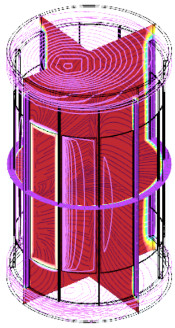
Adjacent	0.012764V	0.014967V	0.018135V	0.022856V	0.031729V
Opposite	6.02E-04V	6.63E-04V	7.35E-04V	8.19E-04V	9.26E-04V
100	Top View				
	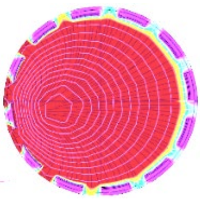	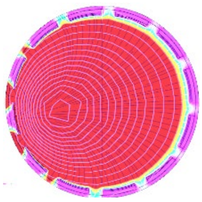	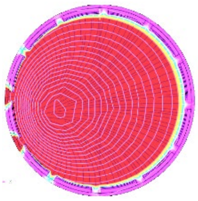	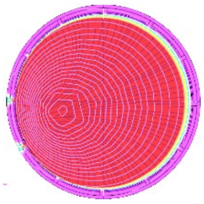	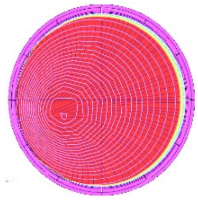
	3D View				
	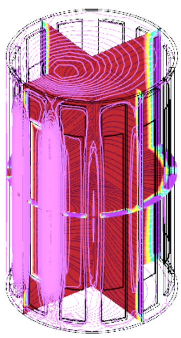	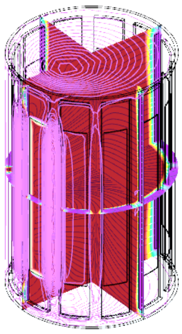	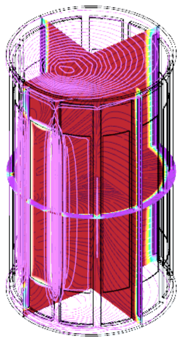	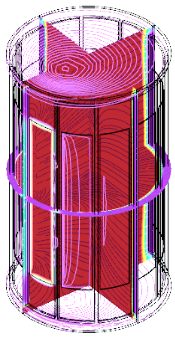	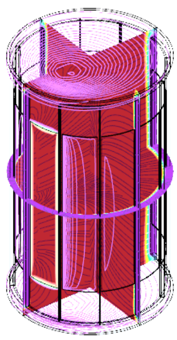
Adjacent	0.012992V	0.015328V	0.018514V	0.02316V	0.032106V
Opposite	6.35E-04V	7.02E-04V	7.80E-04V	8.66E-04V	9.81E-04V
110	Top View				
	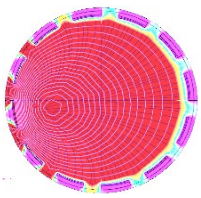	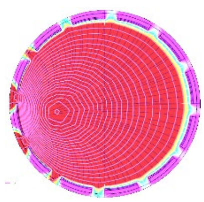	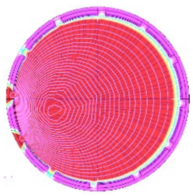	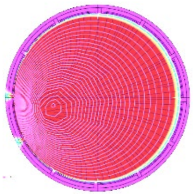	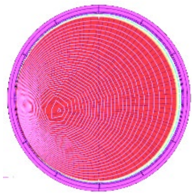

	3D View				
	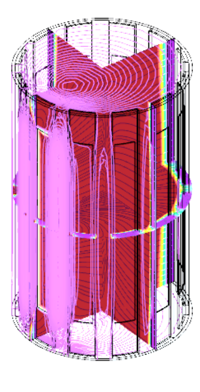	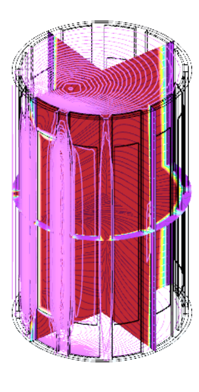	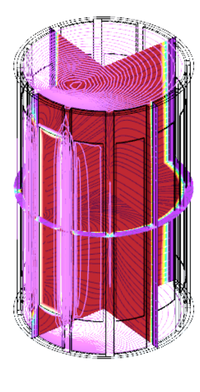	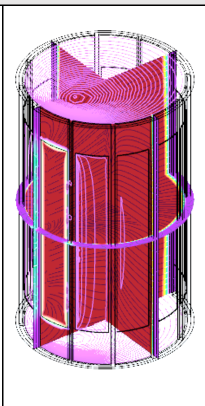	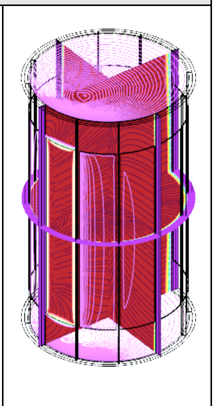
Adjacent	0.013164V	0.015528V	0.018743V	0.02349V	0.032587V
Opposite	6.70E-04V	7.43E-04V	8.24E-04V	9.18E-04V	0.0010388V
	Colour indication bar of homogenous medium:  Low (V) High (V)				

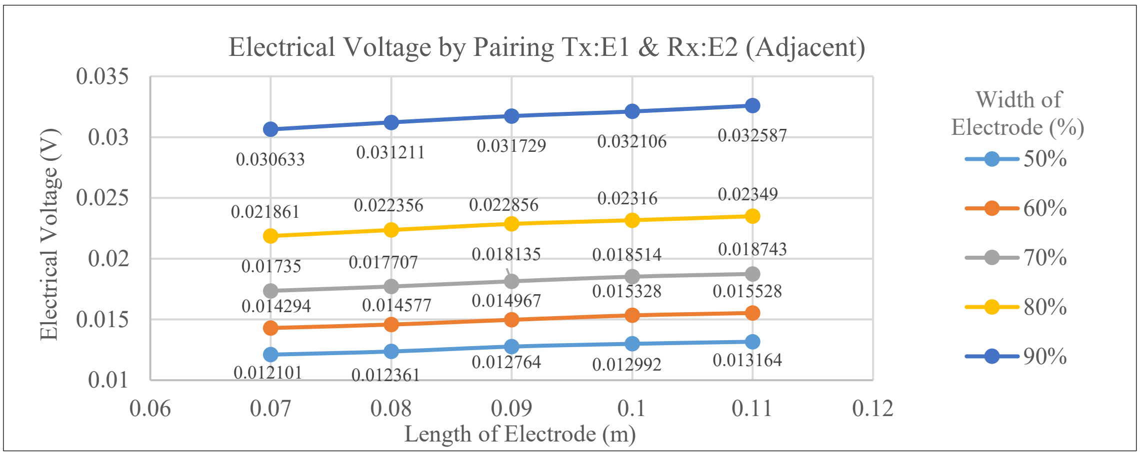

(a)

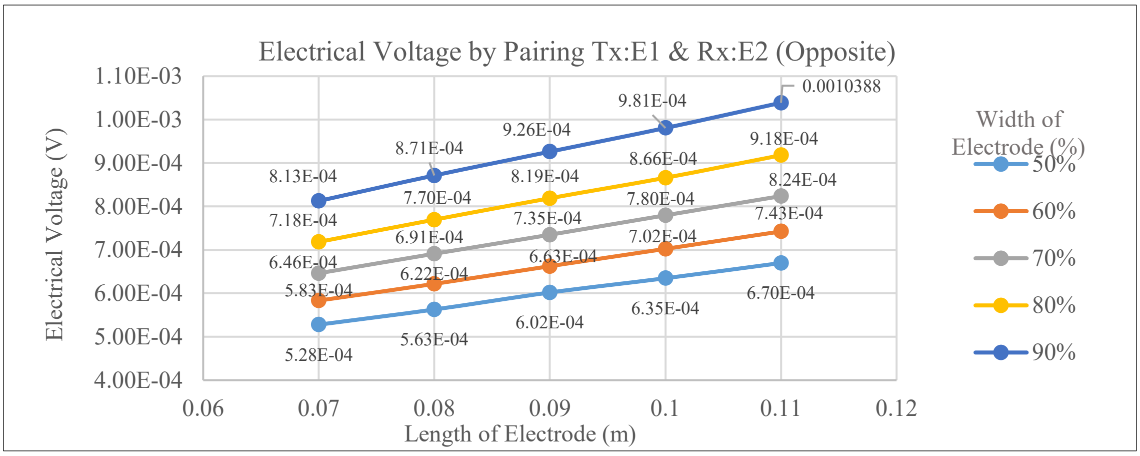

(b)

Figure 5. Electrical voltage versus length of electrode: (a) adjacent readings and (b) opposite readings

From Table 6 and Figure 5, the simulation result using the proposed parameters in this study showed that longer and wider sensors provided higher electrical voltage in a homogenous medium. It is evident that the 90% of width of sensor and length of 110 mm for the electrode represent the optimal sensor diameter for this invasive ECT system. However, based on research by [23], a sensor with invasive electrodes will normally have superior electrical performance to one using non-invasive electrodes, but the design and construction of sensors with invasive electrodes is considered more complex, and therefore will increase the cost of the system.

In light of this, and given the intention to fabricate the sensor, further research was conducted to determine whether to proceed with the archived simulated dimensions or utilize slightly shorter dimensions. Therefore, 80% of the width and 90 mm of the electrode length were tested. To validate these new sensor dimensions, frequency selections were re-simulated to verify the efficiency of 400 kHz under these updated parameters. The article in Ref. [20] was referred. Figure 6 illustrates the frequency graph comparing the previous sensor configurations (90% of sensor width and 110 mm electrode length) with the current configuration (80% electrode width and 90 mm electrode length). The results indicate an unchanged frequency response, confirming 400 kHz as the optimum frequency. Consequently, 400 kHz was selected for the subsequent simulation to identify liquid-gas regimes in the conducting pipe with 80% electrode width and 90 mm electrode length.

Furthermore, to observe a non-homogenous medium, various diameter of phantoms, each with the same length as the pipe, are constructed in the center of the pipe using COMSOL Multiphysics software. The reason for using the center position is because it was well known that obtaining results at the center of the region for electrical tomography is more challenging compared to the positions nearer to the electrode. The diameter of the phantoms ranges from 5 mm to 25 mm in increments of 5 mm. The phantom material is air, and its relative permittivity, ε is 1. The adjacent and opposite measurements are also obtained in this study to observe the electrical voltage distribution and values. Table 7 presents the simulation results of the constructed geometry of the invasive ECT system with various diameters of phantoms in COMSOL Multiphysics software.

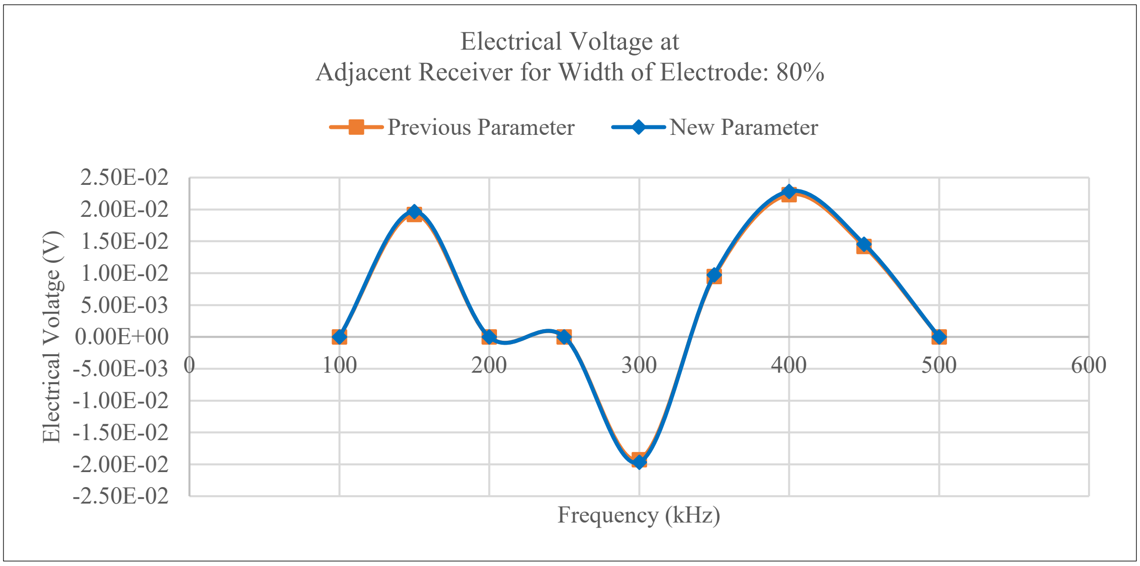

(a)

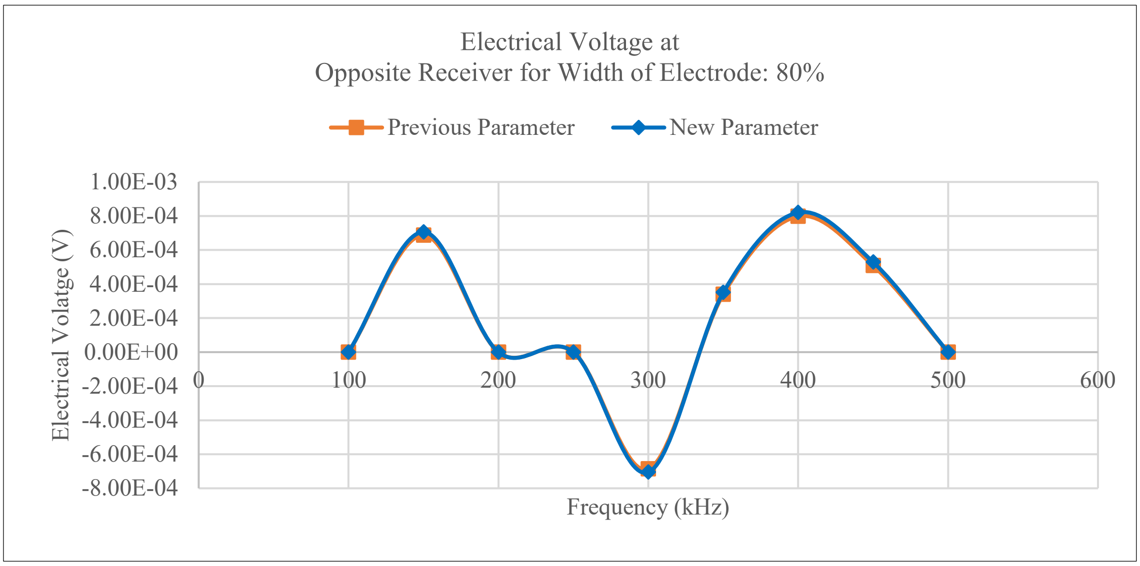

(b)

Figure 6. The new optimum frequency analysis; electrical voltage at (a) adjacent receiver and (b) opposite receiver.

Table 7. Electrical potential distribution and values for non-homogenous conditions by applying different sizes of phantoms using a sensor width of 80% and electrode length of 90 mm.

Phantom Diameter (mm) / Measurement	**3D Geometry**	**3D view**	**Top View**
5	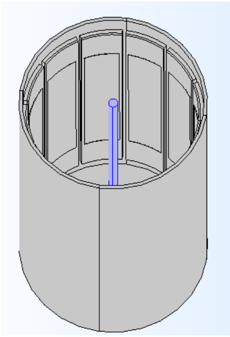	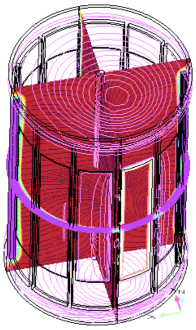	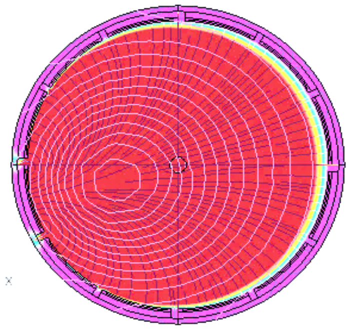
Adjacent	0.022882V		
Opposite	7.79E-04V		
10	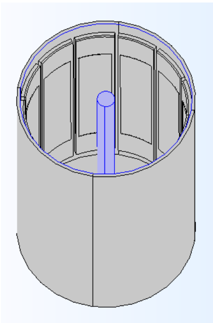	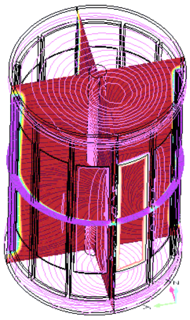	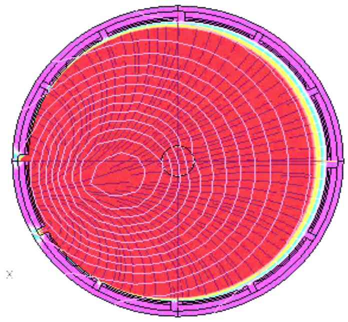
Adjacent	0.023002V		
Opposite	6.75E-04V		
15	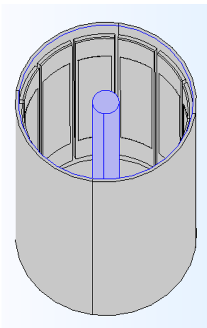	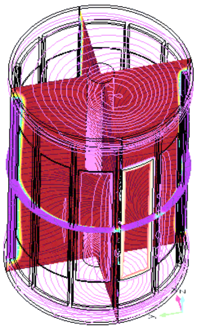	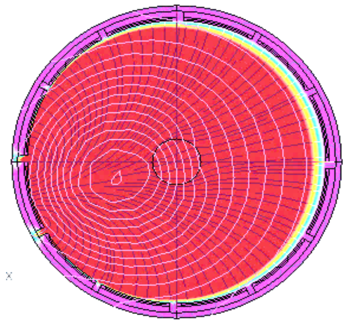
Set A	0.023248V		
Set B	5.39E-04V		
20	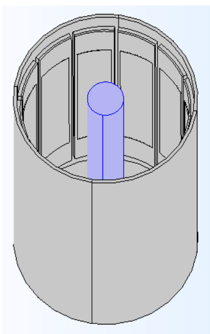	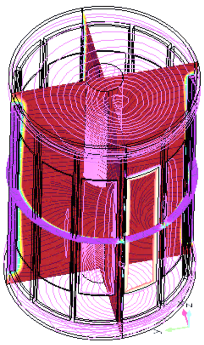	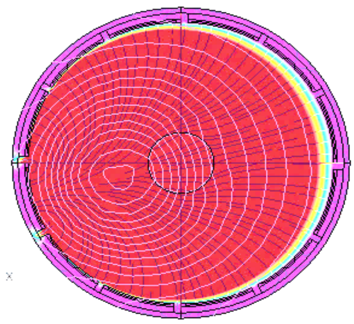
Adjacent	0.023573V		
Opposite	4.12E-04V		
Color indication bar of non-homogenous medium: Low (V) High (V)			

The simulation results at the adjacent electrode indicate that if the diameter of the phantom (mm) increases, the electrical voltage (V) is also increases. Meanwhile, the simulation results for opposite electrode measurement reveals that as the diameter of the phantom (mm) increases, the electrical voltage is decreases. It is also observed that the voltage distribution (multislice line in black and contour line in purple) inside the pipe become more distorted as the phantom size increases. Again, the curving line representing by the multislice also obey the soft field behaviour of the electrical tomography.

In validating the measurement of the simulation model for the invasive ECT system, several tests were conducted to obtain the tomogram of the region of interest. These tests involved varying the sizes and positions of multiple statis gas in the oil medium. The LBP algorithm served as the foundation for image reconstruction. Additionally, the results were enhanced using global thresholding (GT), with an average value of 0.89. The threshold value was chosen based on the averaging for all test profiles with absolute error (AE) closest to +/- 0. Using global thresholding analysis, the new non-homogenous geometries simulation was tested and constructed in 2-Dimensional to facilitate quicker computations and produce efficient simulations of the image reconstruction while retaining the optimum parameters as the previous 3D simulation parameter. To address the disparity of the parameter selection, the decision was made to eliminate the thickness of the insulated layer of the sensor in the construction of the geometry in COMSOL Multiphysics software. The insulated layer was remodelled as a single line, maintaining the same material and relative permittivity are as before. Table 8 displays the tomogram results from testing conducted with MATLAB software to validate the optimized measurements of the 80% electrode width and 90 mm electrode length. To obtain the tomograms, two phantom sizes (10 mm and 20 mm) were used, each positioned at distinct locations.

Table 8. Tomograms obtained for different size, positions and number of tested phantoms.

Test Profile		**Reference Image**	**LBP**	**GT**	
A	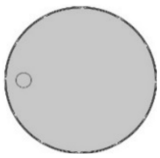	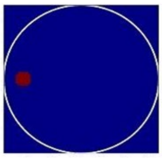	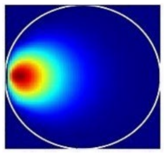	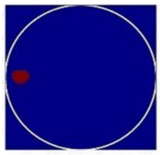	Gas (max.) 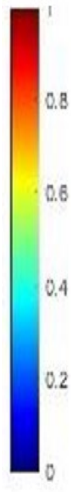 Oil (min.)
B	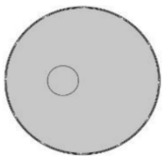	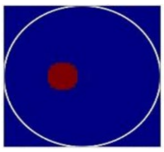	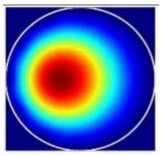	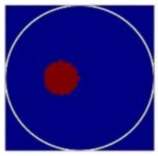	
C	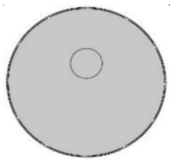	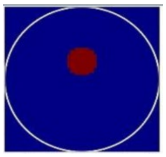	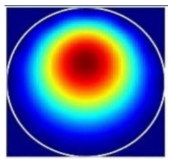	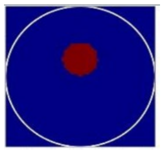	
D	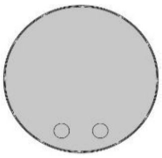	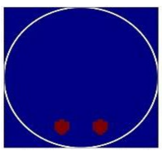	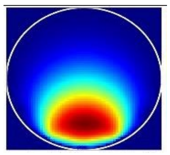	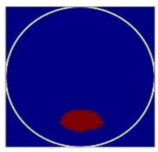	
E	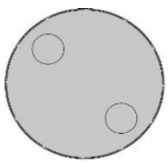	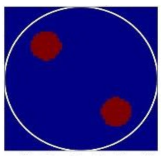	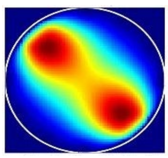	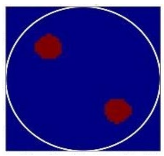	
F	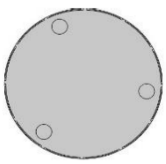	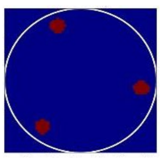	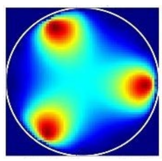	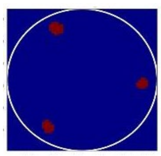	

G	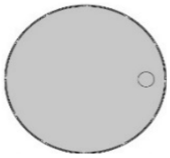	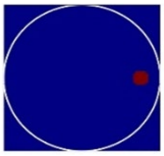	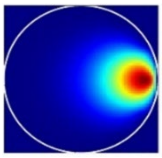	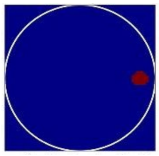	

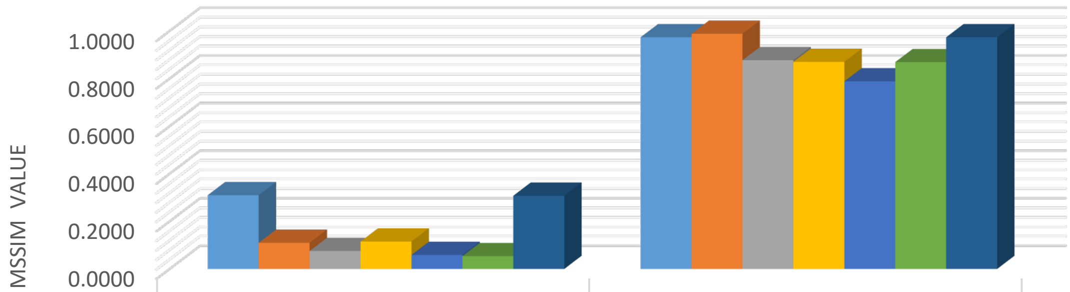

	LBP	GT
A	0.3101	0.9737
B	0.1099	0.9882
C	0.0754	0.8773
D	0.1151	0.8703
E	0.0588	0.7882
F	0.0539	0.869
G	0.3077	0.9737

Figure 7. MSSIM index and bar graph for various test profiles using LBP and GT.

The simulation model was able to generate the tomograms based on Table 8. The tested phantoms' sizes and placements were likewise determined by the algorithm. However, the blurring effect of the LBP algorithm in comparison to the GT technique made it more difficult to distinguish between small and large sizes. Then, the analysis using multi-scale structural similarity (MSSIM) was implemented. It measures how similar local structures or patterns are across a range of image scales. According to [24], if the tomograms' MSSIM value is 1 or very close to 1, the quality or resolution of the image reconstruction is almost identical to the reference image. Figure 7 shows the value of MSSIM index and representing in bar graph for both LBP and GT. It is evident that all phantom locations exhibit poor results from the LBP algorithm, with all phantoms exhibiting low MSSIM values. In general, however, the GT technique outperforms the others, with an average MSSIM value of approximately 0.9058 for the majority of phantoms. Consequently, the GT method outperforms the LBP algorithm, which departs greatly from the reference image.

5. CONCLUSION

In conclusion, this paper presents a comprehensive simulation study aimed at optimizing the dimensions of invasive ECT sensors, specifically focusing on the width and length, to observe dielectric mediums in homogeneous and non-homogeneous conditions within conducting pipes. By conducting a detailed analysis of simulation data from COMSOL Multiphysics software and image reconstruction using MATLAB software, the optimal width and length of the ECT sensor are determined. The simulation results indicate that the sensitivity and resolution of the invasive ECT system are significantly influenced by these dimensions. Optimal sensor dimensions with 80% of sensor coverage area and 60% out of the pipe length provide higher electrical voltage and better resolution for the invasive ECT system. Utilizing the chosen parameters for the invasive ECT sensor, this simulation study successfully produces accurate tomograms, especially for non-homogeneous testing using a different size and location of phantoms and the global threshold technique. The analysis consistently demonstrates that the global threshold method outperforms the LBP algorithm in terms of MSSIM values, reflecting superior image reconstruction. Furthermore, future experimental investigations involving hardware components will be conducted to validate the simulation results and refine the design parameters. Additionally, developing an iterative algorithm for this proposed technique will be a primary focus of our future work.

ACKNOWLEDGMENT AND FUNDING

The authors would like to thank the Ministry of Higher Education, Malaysia for providing financial support under Fundamental research grant No. FRGS/1/2021/TK0/UMP/02/11 (University reference RDU210111) and Universiti Malaysia Pahang Al-

Sultan Abdullah, Malaysia for laboratory facilities as well as additional financial support under Internal Research grant RDU210316.

DECLARATION OF CONFLICTING INTERESTS

The authors declare no potential conflicts of interest with respect to the research and publication of this article.

REFERENCES

[1] W. Deabes and K. E. Bouazza, Efficient image reconstruction algorithm for ECT system using local ensemble transform kalman filter, *IEEE Access*, 9, 2021, 12779–12790.

[2] H. Wang and W. Yang, Application of electrical capacitance tomography in pharmaceutical fluidised beds – A review, *Chemical Engineering Science*, 231, 2020, 116236.

[3] Z. Ji, J. Liu, H. Tian and W. Zhang, ECT sensor simulation and fuzzy optimization design based on multi index orthogonal experiment, *IEEE Access*, 8, 2020, 190039–190048.

[4] B. Liu, C. Tang, K. Tang and H. Hu, A Water fraction measurement method using heuristic-Algorithm-based electrical capacitance tomography images post-processing technology, *IEEE Access*, 8(1), 2020, 206418–206426.

[5] H. Guo, S. Liu, H. Cheng, S. Sun, J. Ding and H. Guo, Iterative computational imaging method for flow pattern reconstruction based on electrical capacitance tomography, *Chemical Engineering Science*, 214, 2020, 115432.

[6] Z. Xu, F. Wu, L. Zhu and Y. Li, LSTM model based on multi-feature extractor to detect flow pattern change characteristics and parameter measurement, *IEEE Sensors Journal*, 21(3), 2021, 3713–3721.

[7] N. A. Zulkiflli, J. Pusppanathan, P. L. Leow, S. M. Din, M. F. Rahmat, Y. K. Wong, F. A. Phang and N. F. A. B. Rahman, Finite element analysis for yeast cells using electrical capacitance tomography, *Proceedings of the 2019 IEEE International Conference on Signal and Image Processing Applications*, Malaysia, 2019, 346–350.

[8] W. Tian, *Electrical Capacitance Tomography with Variable Diameter and Potential Application for Pole Inspection*, Ph.D. Dissertation, University of Manchester, 2017.

[9] W. Yang, Design of electrical capacitance tomography sensors, *Measurement Science and Technology*, 21(4), 2010, 042001.

[10] R. Ramanathan, P. Arulmozhivarman, P. Tatavarti, Optimal design and fabrication steps of electrical capacitance tomography sensors, *Instrumentation Science & Technology,* 41(3), 2013, 301–310.

[11] L. Peng, C. Mou, D. Yao, B. Zhang and D. Xiao, Determination of the optimal axial length of the electrode in an electrical capacitance tomography sensor, *Flow Measurement and Instrumentation*, 16(2–3), 2005, 169–175.

[12] K. Huang, S. Meng, Q. Guo, W. Yang, T. Zhang, M. Ye and Z. Liu, Effect of electrode length of an electrical capacitance tomography sensor on gas-solid fluidized bed measurements, *Industrial and Engineering Chemistry Research*, 58(47), 2019, 21827–21841.

[13] H. S. Hamzah, A. E. Che Man, Y. Abdul Wahab, N. Abu Talip and M. M. Saari, Development of image reconstruction for detecting static oil-gas regimes using invasive electrical capacitance tomography in steel pipe application – an initial study, *Jurnal Teknologi*, 86(3), 2024, 135–143.

[14] William H. Hayt and John A. Buck, *Engineering Electromagnetics*, 7th. ed., New York: McGraw Hill, 2006.

[15] R. Abdul Rahim, *Electrical Capacitance Tomography; Principles, Techniques and Applications*, Penerbit UTM Press, 2011.

[16] B. K. Singh, S. Roy and V. V. Buwa, Bubbling/slugging flow behavior in a cylindrical fluidized bed: ECT measurements and two-fluid simulations, *Chemical Engineering Journal*, 383, 2019, 123120.

[17] S. K. Mohammed, A. H. Hasan, A. Ibrahim, G. Dimitrakis and B. J. Azzopardi, Dynamics of flow transitions from bubbly to churn flow in high viscosity oils and large diameter columns, *International Journal of Multiphase Flow*, 120, 2019.

[18] N. Amizan, A. Rahman, R. Abdul, A. Mohd, L. Pei, J. Pusppanathan and E. Johana, A review on electrical capacitance tomography sensordevelopment, *Jurnal Teknologi*, 3(73), 2015, 35–41.

[19] Y. Abdul Wahab, R. Abdul Rahim, L. Pei Ling, M. H. Fazalul Rahiman, S. Ridzuan Aw, F. R. Mohd Yunus and H. Abdul Rahim, Optimisation of electrode dimensions of ERT for non-invasive measurement applied for static liquid–gas regime identification, *Sensors and Actuators, A: Physical*, 270, 2018, 50–64.

[20] A. E. Che Man, Y. Abdul Wahab, N. Abu Talip, S. Ridzuan Aw, M. M. Saari, R. Abdul Rahim and S. Y. Yu, Simulation of Frequency Selection for Invasive Approach of Electrical Capacitance Tomography for Conducting Pipe Application Using Oil-Gas Regimes, *Proceedings of the 2022 Engineering Technology International Conference*, Malaysia, 2022, 63–68.

[21] M. J. Pusppanathan, N. M. N. Ayob, F. R. Yunus, S. Sahlan, K. H. Abas, H. A. Rahim, R. A. Rahim and F. A. Phang, Study on single plane ultrasonic and electrical capacitance sensor for process tomography system, *Sensors and Transducers*, 150(3), 2013, 40–45.

[22] L. Peng, J. Ye, G. Lu and W. Yang, Evaluation of effect of number of electrodes in ECT sensors on image quality, *IEEE Sensors Journal*, 12(5), 2012, 1554–1565.

[23] R. Abdul Rahim, Z. C. Tee, M. H. Fazalul Rahiman and J. Pusppanathan, A low cost and high speed electrical capacitance tomography system design, *Sensors & Transducers*, 114(3), 2010, 83–101.

[24] Z. Wang, A. C. Bovik, H. R. Sheikh and E. P. Simmoncelli, Image Quality Assessment: From Error Visibility to Structural Similarity, *IEEE Transactions on Image Processing*, 13(4), 2004, 600–612.